Size and surface-engineered $BiVO_4$ catalytic smooth spheres for efficient electrochemical detection of bifenox herbicide

Thangaraju Dheivasigamani,[1]* Kumaravel Ammasai,[2]* Priyadharshini Shanmugam,[1] Govarthini Seerangan Selvam,[1] Durairajan Arulmozhi,[3]

[1]*nano-crystal Design and Application Lab (n-DAL), Department of Physics, PSG Institute of Technology and Applied Research, Coimbatore-641062, Tamil Nadu, India*

[2]*Functional Materials Lab (FML), Department of Chemistry, PSG Institute of Technology and Applied Research, Coimbatore-641062, Tamil Nadu, India*

[3]*I3NAveiro, Department of Physics, University of Aveiro, 3810 193 Aveiro, Portugal*

Corresponding author

*E-mail: dthangaraju@gmail.com (Thangaraju Dheivasigamani)

*E-mail: kumaravel@psgitech.ac.in (Kumaravel Ammasai)

Abstract

Smooth surface and periodic size control synthesis of $BiVO_4$ semiconducting particles were achieved under hydrothermal conditions with long carbon chain oleic acid as an additive in weak organic acid and methanol as solvents for bifenox, a nitrodiphenyl ether herbicide detection. The conventional hydrothermal synthesis of $BiVO_4$ has a rough surface and hierarchical morphology. The current method gives a way to provide smooth and tuned particle size. The structure and morphology of the derived $BiVO_4$ under various concentrations of oleic acid were characterized by X-ray diffraction, Raman, and Scanning Electron Microscopy analysis. A glassy carbon electrode (GCE) modified with $BiVO_4$ nanoparticles was applied to determine bifenox electrochemically. Since bifenox is a nitroaromatic herbicide, the electrochemical parameters of bifenox herbicide detections were carried out using nitrophenol as a model compound using Cyclic Voltammetry (CV). Sensing characterizations are carried out with Differential Pulse Voltammetry (DPV) and Amperometry techniques. Bifenox undergoes electrochemical reduction at -500 mV on $BiVO_4$ modified electrode, and the limit of detection (LOD) was found to be 0.3 nM. Hence, the practical accessibility of the present $BiVO_4$-modified GCE was good for the environmental analysis of bifenox herbicide.

Keywords: $BiVO_4$ spheres, electrochemical detection, nitrophenol, bifenox, Cyclic voltammetry

1. Introduction

Bismuth-based catalytic materials have attracted considerable interest due to their great potential for adsorption and inherent reducibility.[1–3] Bismuth tungstate[4], bismuth molybdate,[5,6] and bismuth dichalcogenides[7] have all gained significant attention in research and development among bismuth-based nanostructures due to their efficient photocatalytic activity, good stability, distinctive optical band gap, and high dielectric strength. Among them, the Bi-V-O series phases, which comprise $BiVO_4$, $Bi_4V_2O_{11}$, $Bi_{25}VO_{40}$, and $Bi_{46}V_8O_{89}$, possess unique properties to employ in many practical applications.[8,9] In addition, bismuth functions as a traditional submetallic material of the vanadium (V) group and possesses several unique characteristics, including low carrier concentration, a highly non-isotropic Fermi surface, and an extended carrier lifetime.[10,11] Bismuth vanadate ($BiVO_4$), a standard Bi-V-O system, is an n-type semiconductor[12,13] that has been widely developed as an effective functional material because of its exceptional qualities, including its narrow band gap, resilience to corrosion, good dispersibility, non-toxicity, and high photocatalytic performance.[14,15] Also, it is a strong contender for solar light harvesting due to its flexible optical and electrical features with a band gap of 2.4 eV.[16,17] Notably, there are only three crystalline phases where $BiVO_4$ may be found most commonly, and they are zircon–tetragonal (z–t), scheelite–tetragonal (s–t), and scheelite–monoclinic (s–m).[18] The irreversible phase shift from tetragonal to monoclinic scheelite happens around 670-770 K.[19] In addition, it has been ascertained that only the scheelite-monoclinic (s-m) crystal structure is particularly active under visible light as it has the ideal band location to capture visible light from the sun and is also capable of having antibacterial properties.[20,21] The scheelite monoclinic structure of $BiVO_4$ contains a vanadium ion linked by four oxygen atoms in a tetrahedral site. The bismuth ion is attached to eight oxygen atoms from eight different VO_4 tetrahedral units.[22] Owing to its unique properties, $BiVO_4$ has

practical utility in the pigment industry, electronic devices, the catalytic destruction of hazardous contaminants, and the electrocatalytic reduction of pollutants. Especially, $BiVO_4$ was recognized as potential semiconducting material due to the specific overlapping of the Bi_{6s} and O_{2p} orbitals as well as the contribution of the Bi^{3+} lone pair to raising the energy level to the top of the conduction band (CB), which causes a reduction in the semiconductor band gap offering advantageous to the mobility of generated charge carriers (B5).[23,24] $BiVO_4$ has been prepared using a number of techniques, including solid-state reactions,[25] co-precipitation,[26] hydrothermal processes[27] and sonochemical routes.[28] Of the various paths, hydrothermal synthesis is a soft-chemical method that is frequently employed in the preparation of many different types of effective materials.[29,30] Also, this technique makes it simple to regulate the form and size of the synthesized nanostructure.[31]

In account of various toxic environmental pollutants, herbicides are a type of compound that is extensively used to manage undesired vegetation. They are commonly employed in forestry, agriculture, grazing systems, and urban green zones.[32] Herbicide contamination may harm creatures that are critical components of the food chain, such as primary producers, which form the foundation of the food chain for aquatic animals.[33] In this context, Bifenox (methyl 5-(2,4-dichlorophenoxy)-2-nitrobenzoate), a selective herbicide that is used to suppress annual broad-leaved weeds in a variety of crops, including cereals, maize, soybeans, rice, and many more. It is often identified in aquatic environments at dangerous concentration levels for aquatic animals.[34] Monitoring the bifenox herbicide level in the environmental samples is necessary. The herbicides and pesticides are routinely analyzed using HPLC,[35] GC,[36] GCMS,[37] and LCMS.[38] However, these instruments are expensive and not readily available everywhere. It is the need of the hour to develop low-cost, portable, and sensitive instruments for detecting herbicides in the environment. Electrochemical methods are more suitable because of their low-cost, portable instruments that

can be designed and are highly sensitive.[39] The major problem associated with the electrochemical detection sensitivity is the working electrode's surface. Coating suitable catalytic materials improve the sensitivity of the working electrode surface over the surface.[40] However, there is scarce data on the electrochemical detection of bifenox herbicide. The as-synthesized $BiVO_4$ nanoparticles modified for the electrochemical detection studies of Bifenox indicate its possibility in herbicide detection.

In this work, novel size and surface-controlled spheres of $BiVO_4$ were synthesized by hydrothermal method. The present work is considered the first to employ BiVO4 nanoparticles to detect bifenox herbicide. A systematic study was carried out to investigate the detection in water samples. XRD, Raman, SEM, XPS and TEM analysis analyzed the structure and surface morphology. The determination of bifenox has been investigated using prepared electrode material by employing techniques such as cyclic voltammetry (CV), differential pulse voltammetry (DPV), and Amperometry.

2. Experimental Methods

2.1. Materials

Bismuth nitrate pentahydrate ($Bi(NO_3)_3 \cdot 5H_2O$), vanadyl acetylacetonate ($VO(C_5H_7O_2)_2$), glacial acetic acid (CH_3COOH), Oleic acid ($C_{18}H_{34}O_2$) and methanol (CH_3OH) were used as purchased. Nitrophenol and bifenox herbicide were purchased from Merck Life Science Pvt Ltd, and a stock solution of bifenox (3800 µM) was prepared in methanol solvent. This stock solution was diluted with Britton- Robinson buffer having pH 2.5 and used as an analyte. The B–R buffer solution was prepared by adding 15 ml of 0.2 M sodium hydroxide solution into 100 ml of a mixed acid containing 0.04 M of each boric, orthophosphoric, and acetic acid. The desired pH was

achieved by adding HCl or NaOH solutions. All other reagents used were of analytical reagent grade.

2.2. Synthesis of $BiVO_4$ nanoparticle

The synthesis of $BiVO_4$ was performed through the hydrothermal method. The hydrothermal method was chosen for $BiVO_4$ synthesis since at only high temperatures; the reaction occurs so that control can be achieved, thus making an effective synthesis route for $BiVO_4$ formation. The schematic representation of the synthesis of $BiVO_4$ is presented in Figure 1. For the $BiVO_4$ synthesis, a beaker dissolved 0.242 g of bismuth nitrate pentahydrate in 10 ml of acetic acid. Similarly, 0.132 g of vanadyl acetylacetonate was dissolved in 65 ml of methanol in a separate beaker and stirred for complete dissolution. Both solutions are mixed and stirred until fundamental particles completely dissolve, resulting in a colorless solution. The as-prepared solution was transferred to a Teflon-lined autoclave (100 ml) and kept inside a vacuum oven at 170 °C for 16 h. The obtained solution was observed to be golden yellow which was then cooled, centrifuged at 3500 rpm for 5 min each, and collected. Similarly, different concentrations of oleic acid viz 0.5, 1, and 1.5 ml were added to the obtained solution of $BiVO_4$ and stirred thoroughly without dissipation for about 10 min, and process mentioned above was carried out.

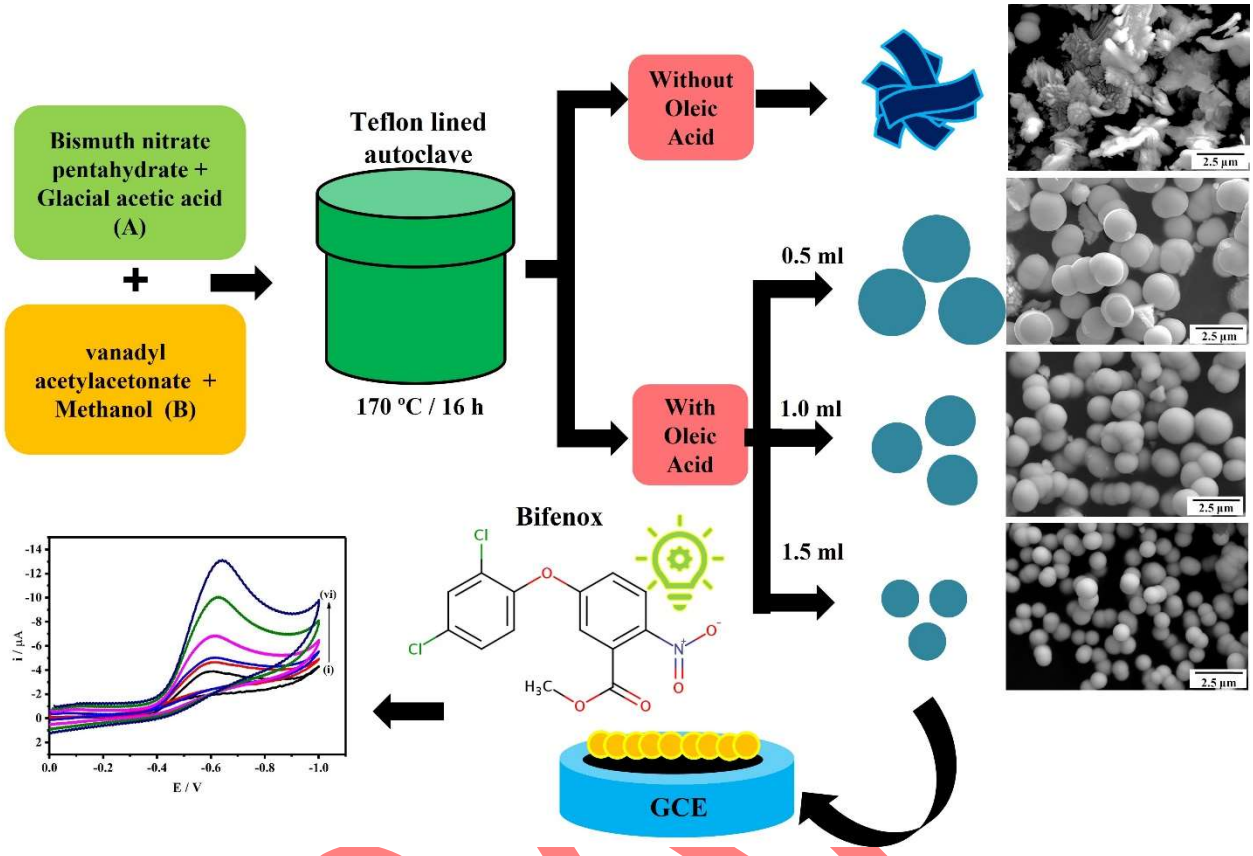

Figure 1. Schematic diagram of the synthesis of $BiVO_4$ smooth-size controlled spheres

2.3. Characterization

The structural studies of $BiVO_4$ were analyzed using Philips PANalyticalXpert pro powder X-ray Diffractometer with Cu Kα (1.54 Å). The Raman spectral analysis was employed using a Jobin Yuvon HR 800 Raman spectrometer with a 532nm laser source. The morphological analysis was investigated using Hitachi S-3400N FE-SEM.

2.4. Apparatus for electrochemical sensing

A potentiostat/galvanostat (model SP150) of BioLogic Science Instruments, France was used to perform all the electrochemical sensing experiments. A three-electrode cell set up the working, counter, and reference electrodes used were bismuth vanadate coated GCE (Alfa Aesar3mm diameter), platinum foil, and Ag/AgCl, respectively. A glass cell with a 10 ml capacity

was used to perform all the electrochemical experiments. The electrochemical studies were performed at a temperature of 30 ±1 ºC, and the dissolved oxygen content of the solution was eliminated by purging pure argon for 15 min.

2.5. Preparation of bismuth vanadate modified GCE

The surface of the GCE was mechanically polished using alumina slurry until a mirror-like surface was obtained. Then the electrode was rinsed thoroughly with doubly distilled water, cleaned successively in 10% NaOH solution, 1:1 HNO_3–H_2O (v/v), and methanol each for 2 min and dried in atmospheric air. Bismuth vanadate-modified electrode was prepared by coating 5 µL of the suspension of bismuth vanadate on GCE by simple drop dry method. The modified GCE was dried and employed for all electrochemical experiments in this present study.

3. Results and Discussion

3.1. XRD analysis

The XRD patterns of $BiVO_4$ particles synthesized without and with various quantities of Oleic acid (0.5 ml, 1 ml, and 1.5 ml) are shown in Figure 2. The results indicate the high crystalline nature of $BiVO_4$ with sharp, well-defined peaks.[41] XRD reflections appeared well matched with monoclinic structure (JCPDS No: 00-014-0688).[42] Particle growth in the presence of oleic acid shows considerable changes in the XRD pattern. Crystalline peak sharpness of Oleic acid-grown particles appears with the significant broadening of peaks upon increasing the amount of oleic acid. Oleic acid is an fatty acid surfactant. Generally the use of water insoluable surfactant such as oleic acid produces a narrow sized particles[43]. Herein, the increase in concentration of oleic acid results in broadend peaks of XRD spectra. This shows that increasing the concentration of oleic acid decreases its crystallinity, paving the way for reducing the particle size.

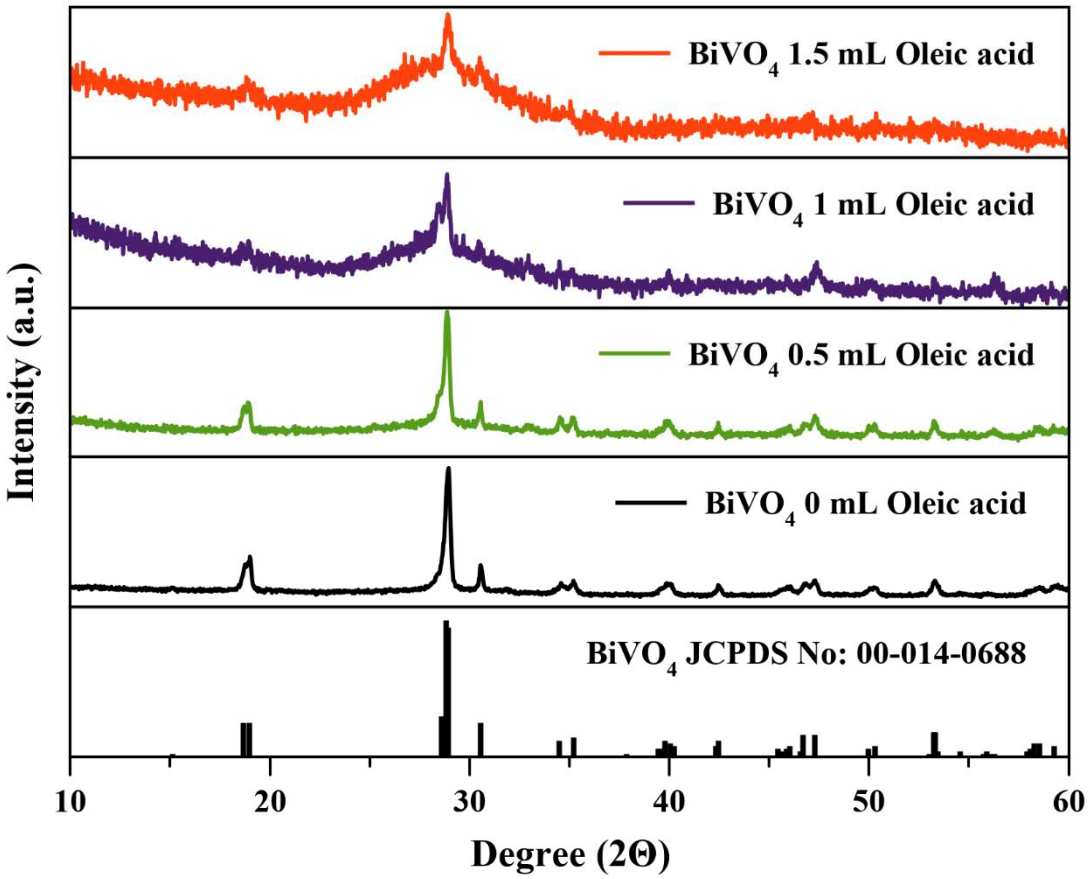

Figure 2. XRD patterns of $BiVO_4$ without oleic acid and with various quantities of Oleic acid (0.5, 1, and 1.5 ml)

3.2. Raman analysis

The direct tool to know about the structural formation and also a sensitive method for the investigation of the crystallization, local structure, and electronic properties of materials was Raman analysis. The Raman spectra of hydrothermally synthesized without and with different concentration of cape agent $BiVO_4$ is shown in Figure 3. The observed Raman spectra show six Raman bands, subdivided into two external (below 250 cm-1) bands and four internal (above 300 cm^{-1}) bands. The asymmetric and symmetric deformation bands of the VO_4^{3-}tetrahedron were observed at 329 and 366 cm^{-1}.[44] The Raman bands at 710 and 826 $cm^{-1}$was attributed to the

stretching modes of two types of V–O bonds A_g symmetry.[45] The Remaining two bands at 211 and 129 $cm^{-1}$was correspond to external(translation/rotation) vibration.[46] Among these vibrational modes, the two stretching vibration bands were observed at 710 and 826 cm^{-1}, providing interesting information on the structural variations due to shape and size changes. The size and shape changes were immediately reflected in the two bands' width and relative intensity.

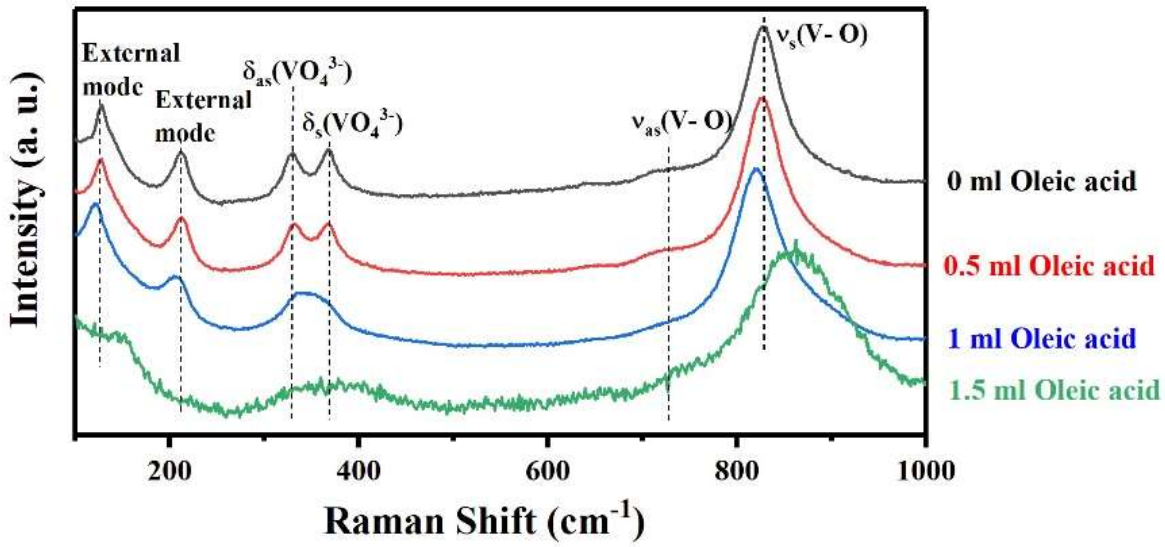

Figure 3. Raman analysis of $BiVO_4$ without oleic acid and with various quantities of Oleic acid (0.5, 1, and 1.5 mL).

The variations in the bond length of the V−O due to the shift could be correlated, which can be calculated by means of an equation. The Raman stretching frequencies and the respective metal−oxygen bond lengths have an inverse relationship. A higher stretching frequency corresponds to a lower metal−oxygen bond length. If the following expression for the bond length was utilized,

$$\vartheta\ (cm^{-1}) = 21349\ e^{-1.9176\ R(Å)} \ldots\ldots\ldots\ldots\ldots\ldots\ldots\ldots..(1)$$

Where *v* is the stretching Raman frequency for V−O, it can be seen that the bond length varies over a range of 1.6938−1.67367 Å for the 0- 1.5 ml oleic acid added samples, respectively. The bond length comparison of V-O with various synthesis methods was compared in Table 1.

Table 1. Symmetry stretching Raman shift and V-O bond length variation with different oleic acid concentrations included $BiVO_4$ synthesis

S.No.	Sample name	Symmetry stretching Raman shift V−O [cm^{-1}]	Bond length V−O [Å]
1	$BiVO_4$ 0 mL Oleic acid	829.43	1.6938
2	$BiVO_4$ 0.5 mL Oleic acid	824.60	1.69684
3	$BiVO_4$ 1 mL Oleic acid	819.76	1.69991
4	$BiVO_4$ 1.5 mL Oleic acid	862.07	1.67367

The Raman analysis of pure $BiVO_4$ and with various quantities of Oleic acid (0.5 ml, 1 ml, and 1.5 ml) are represented in Figure 3. The results annotate the same changes that are observed in XRD patterns. The shift in peaks was observed with an increase in acid concentration. The pure $BiVO_4$ has its major peaks at 340,370,715 and 830 cm^{-1} and ascribes the typical symmetric and anti-symmetric bending modes of vanadate anion. The 830 cm^{-1} also shows the symmetric stretching mode of V-O bonds.

Similarly, 715 cm^{-1} specifies the anti-symmetric V-O stretching mode. The small shoulder peak at 210 cm^{-1} indicates the appearance of an external mode. The rise in the plateau region from 400-750 cm^{-1} in pure $BiVO_4$ with adding 0.5 ml of oleic acid shows a slight decrease in the plateau from 430-620 cm^{-1}. In 1ml of oleic acid, the preferred peaks at 340 and 370 cm^{-1} appeared as a single peak at 350 cm^{-1}. The addition of oleic acid thereby reduces the intensity of peaks as well. To 1.5 ml of oleic acid in $BiVO_4$, significant deformation in peaks with reduced intensity and a peak shift to 870 cm^{-1} was observed.

Raman spectra to harvest the peak positions and the full width at half maximum (FWHM) of the most intensive bands near 819 cm^{-1}. With the increasing concentration of oleic acid, the peak shifts (FWHM) were extracted from fitting 826 (36.79), 819 (46.49), and 860 (68.79) cm^{-1} for 0.5, 1 and 1.5 mL oleic acid. The corresponding FWHM of the peaks was increased with the concentration. The Raman band at 819 cm^{-1} position was more sensitive with short-range order, and width was more sensitive with a degree of crystallinity, defects and disorders, particle size or aggregation of particles. The present case noticed that the oleic acid capping distorted the local symmetry and affected the crystallinity of the compounds. With the increasing oleic acid concentration, the peak position was changed, and the FWHM maximum of the increases indicates the decreasing crystallinity. The same trends were observed in bending modes also. Therefore, the Raman analysis reveals that the samples prepared with lower oleic acid consisted of VO_4 tetrahedra of less symmetric compared with those prepared at higher concentrations of oleic acid. The lower-concentration synthesized samples contained lesser defects and better crystallinity than samples prepared at higher concentrations.

3.3 XPS Analysis

The surface chemical composition and chemical state of the synthesized $BiVO_4$ 1.5 mL Oleic acid sample were identified using XPS. The survey spectrum (Figure 4a) implies that the synthesized sample contains Bi, V, and O. The Bi 4f spectra of $BiVO_4$ 1.5 mL Oleic acid depicted in Figure 4b exhibits two intense peaks at 164.1 eV and 158.8 eV that corresponds to Bi $4f_{5/2}$ and Bi $4f_{7/2}$. This confirms the presence of Bi with +3 oxidation state[47]. The peaks at binding energies of 524 eV and 516.5 eV of V 2p spectra (Figure 4c) that corresponds to V $2p_{1/2}$ and V $2p_{3/2}$ verify the existence of V^{5+} [48]. Three primary peaks can be seen in the XPS spectrum of O 1s presented in Figure 4d. The peak at 529.7 eV is attributed to the lattice oxygen in $BiVO_4$, while the peaks at 531.9 eV and 532.1 eV represent signals from hydroxyl groups of the sample[49].

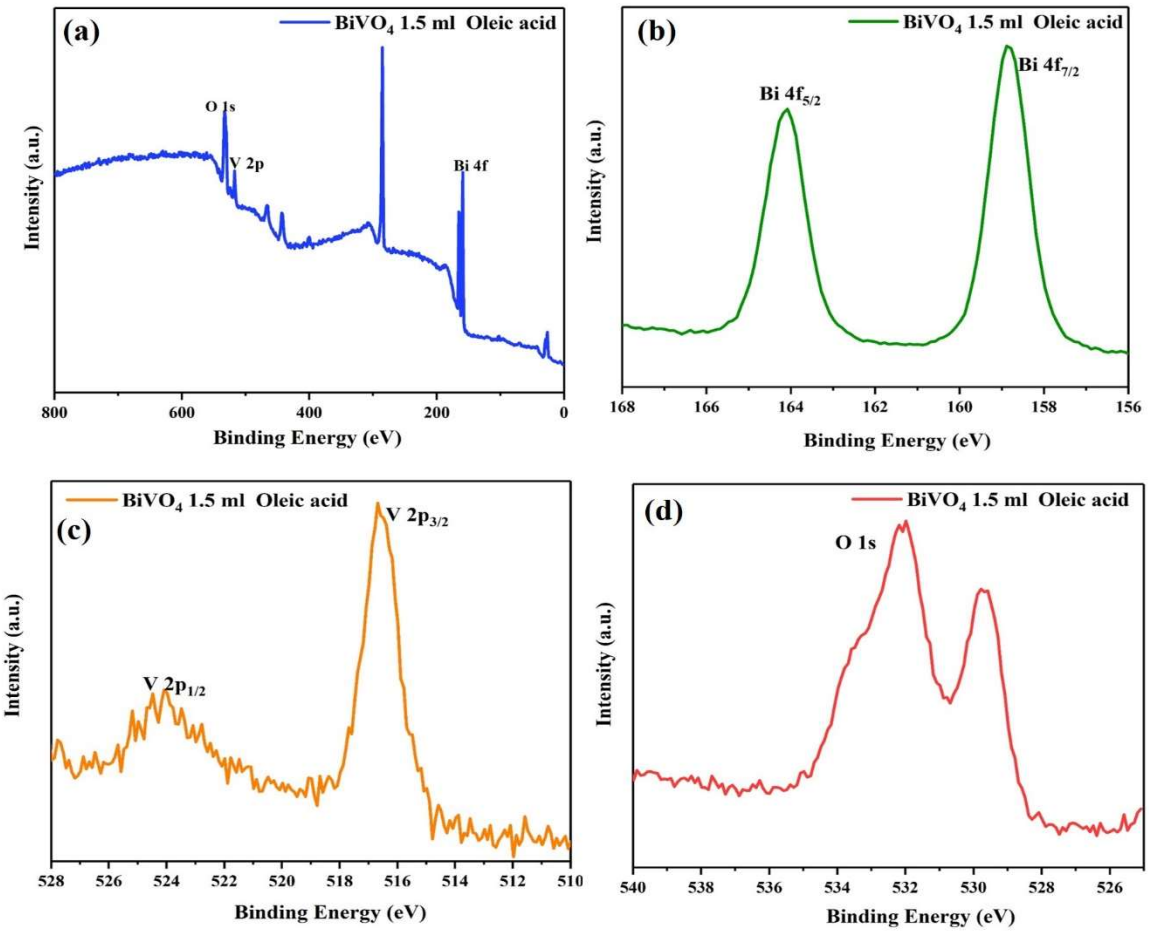

Figure 4. XPS graphs of (a) survey spectrum, (b) Bi 4f, (c) V 2p, (d) O 1s for $BiVO_4$ with 1.5ml oleic acid.

3.4 SEM Analysis

The surface morphology analysis of as-prepared $BiVO_4$ with an adequate quantity of oleic acid compositions (0 ml (a and b), 0.5 ml (c and d), 1 ml (e and f), 1.5 ml (g and h)) were depicted in Figure 5. The change from its typical as a far hierarchical structure to spheres is observed with the addition of oleic acid. The size of perfectly smooth spheres due to oleic acid presence tends to decrease gradually. Thus with the addition of 1.5 ml oleic acid, the size of the particles gradually reduced and appeared as smooth clusters. The appearance of spheres with complete rid of usual hierarchical structures shows the novelty of using oleic acid as an additive to $BiVO_4$. The size of the BiVO4 particles was measured and compared as a histogram presented in Figure 6. The histogram confirmed that 0.5, 1, and 1.5 mL oleic acid introduced $BiVO_4$ particles sized 1500, 1300, and 800 nm, respectively. Fine-tuning of size is possible with this synthesis methodology.

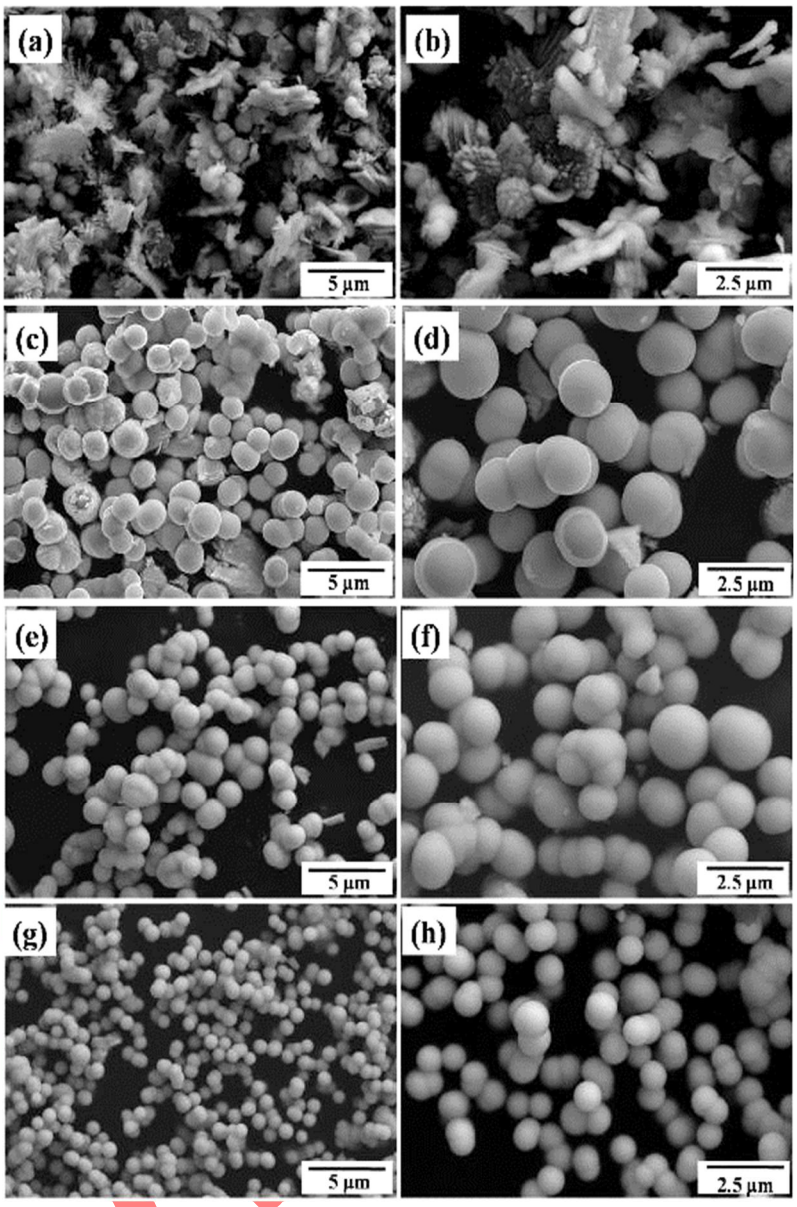

Figure 5. SEM images of $BiVO_4$ without oleic acid (a and b) and with various quantities of Oleic acid (0.5 mL (c and d), 1 mL (e and f), and 1.5 mL (g and h)).

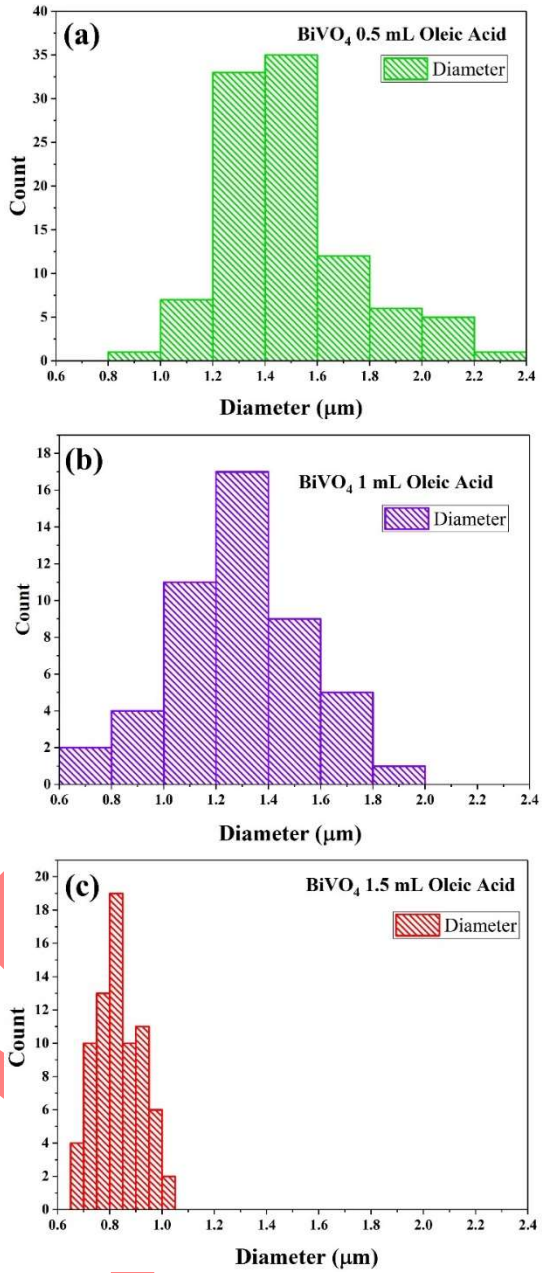

Figure 6. Particle size histogram of synthesis $BiVO_4$ particles from SEM analysis

3.5 TEM analysis

The surface formation of $BiVO_4$ was investigated further using TEM analysis. The TEM images of $BiVO_4$ with 1.5 ml oleic acid at various magnifications are shown in Figure 7 (a-d) . The spherical shape of $BiVO_4$ nanoparticles was observed in TEM images. The particles appear to

be uniform and regular in shape. This confirms that adding oleic acid tunes the BiVO4 particles resulting in a sphere shape for BiVO4 1.5 ml oleic acid, which agrees with SEM analysis.

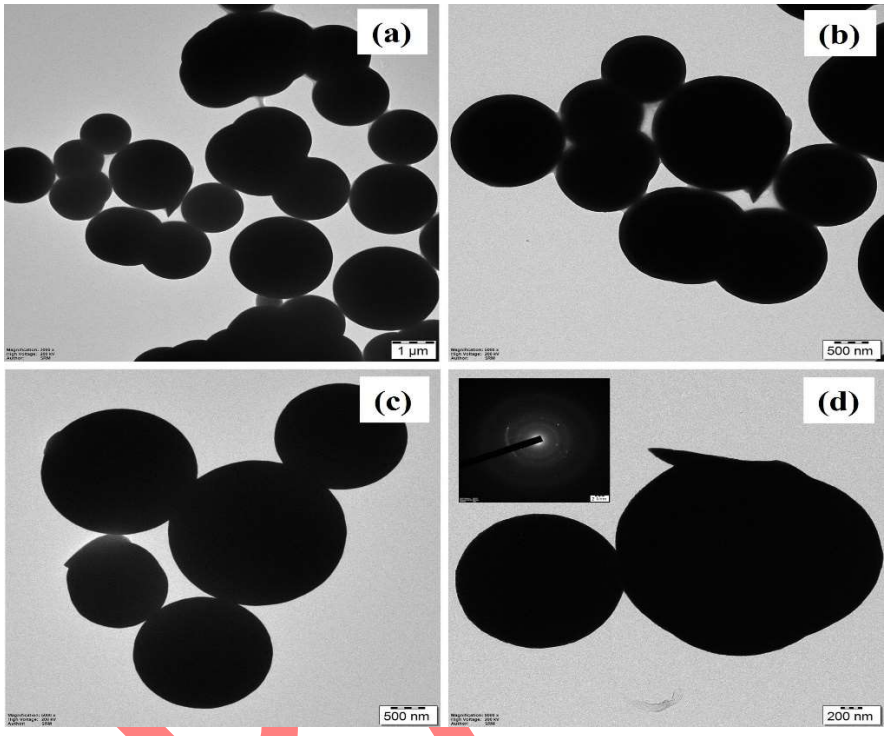

Figure 7. TEM and HRTEM images of $BiVO_4$ with 1.5 mL oleic acid

Figure 8 shows the possible growth mechanism of $BiVO_4$ spheres in the presence of oleic acid. At high temperatures, methanol reacts with acetic acid in an acidic environment (oleic acid) and forms methyl acetate with water as a reaction byproduct. In this condition, formed methyl acetate might create microemulsion spheres in a methanol-water solution and was stabilized by oleic acid surfactant, like that solution without oleic acid less possible to form a methyl acetate in the solution so that the growth of $BiVO_4$ leads shape fewer particles. Once oleic acid is added to the solution forms an acidic environment which helps us to form methyl acetate. An increase in

oleic acid content makes the stabilization of the emulsion smaller in size and leads to controlled particle size.

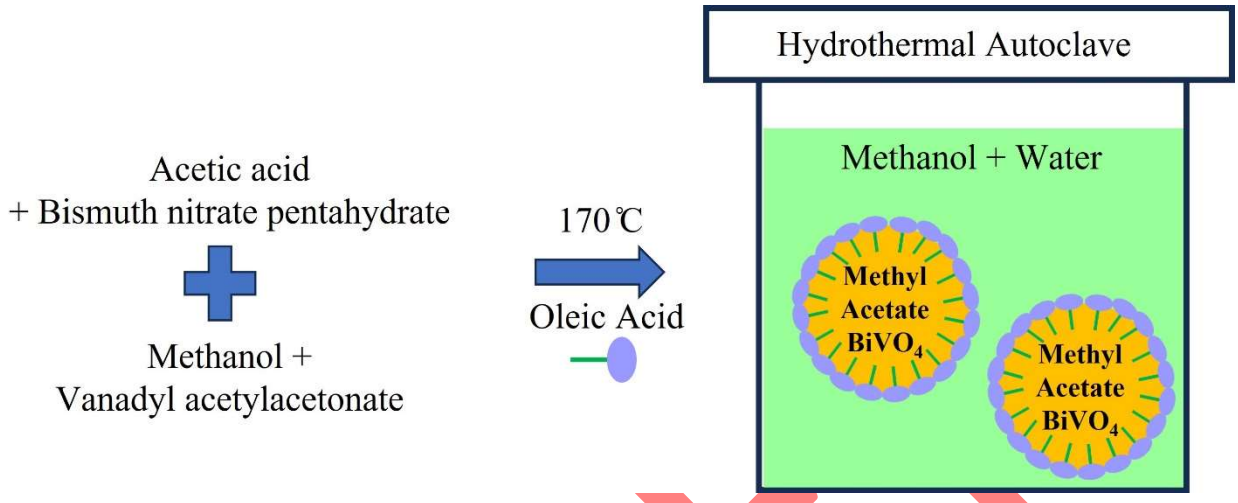

Figure 8 Possible Growth mechanism of $BiVO_4$ sphere formation

3.6. Experimental parameters optimization

The volume of $BiVO_4$ suspension used to modify the GCE surface was optimized using cyclic voltammetry. From Figure 8(a), it can be seen that the peak current is increased if the volume of the modifier is increased up to 5 µL. A further increase in suspension volume has a negative effect on peak current. Therefore, 5 µL of suspension is used to modify GCE surfaces. The pH of the background electrolyte might also influence the electrochemical response of bifenox has been carefully optimized and shown in Figure 8(b). The higher peak current was obtained at highly acidic pH ranges.[50] As pH increases, the current value decreases, so all electrochemical research was conducted at 2.5 pH.

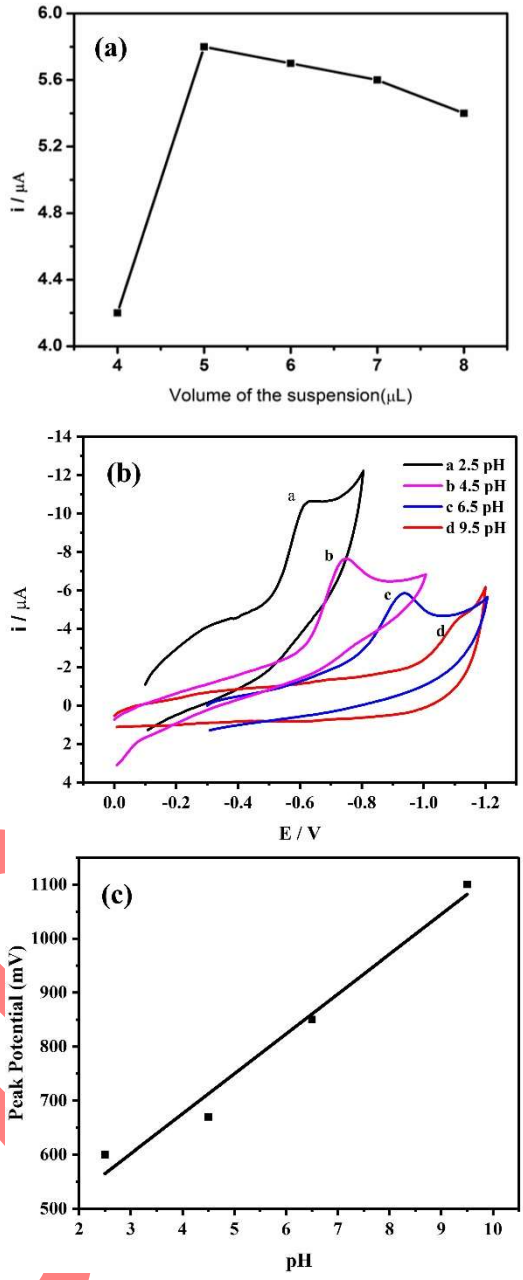

Figure 8. Plot for (a) volume of the modifier vs. peak current, (b) pH vs. peak current, and (c) Plot of peak potential vs. pH with 10 μM concentration of bifenox at sweep rate 100 mVs^{-1}.

3.7. Electrochemical detection of bifenox herbicide

The catalytic properties of the synthesized bismuth vanadate nanoparticles were first assessed on the 4-nitrophenol since both nitrophenol and bifenox belong to the nitroaromatic family of compounds. A cyclic voltammetric method (CV) was used to examine the electrochemical response of nitrophenol on bare GCE and bismuth vanadate-modified GCE with different nano-size particles with and without nitrophenol in 2.5 pH B-R buffer solutions at 100 mV/s. The cyclic voltammetric response of nitrophenol at bare and modified electrodes is shown in Figure 9. Nitrophenol is reduced at about 600 mVs^{-1} on bismuth vanadate-modified GCEs (Figure 9(b-e)) and bare GCE (Figure 9a). However, the reduction current observed on bare GCE is much lower than that observed on bismuth vanadate-modified electrodes. In developing a sensor, the sensing current is one of the most important characteristics. The particle size of BiVO4 plays a vital role in the electrocatalytic reduction of nitrophenol. Sensing currents change considerably with particle size decreasing from 1500 to 800 nm. Compared to other electrodes studied, $BiVO_4$ nanoparticles with sizes of 800 nm possess superior electrocalytic properties. The increased sensing current achieved with these $BiVO_4$-modified electrodes would be useful for detecting trace levels of compounds in the environment. Additionally, as can be seen in Figure 9, the size of the particles decreased, and the reduction potential of nitrophenol shifted to the anodic direction, which also corroborates the superior electrocatalytic property of smaller-sized $BiVO_4$ particles towards the reduction of nitrophenol.

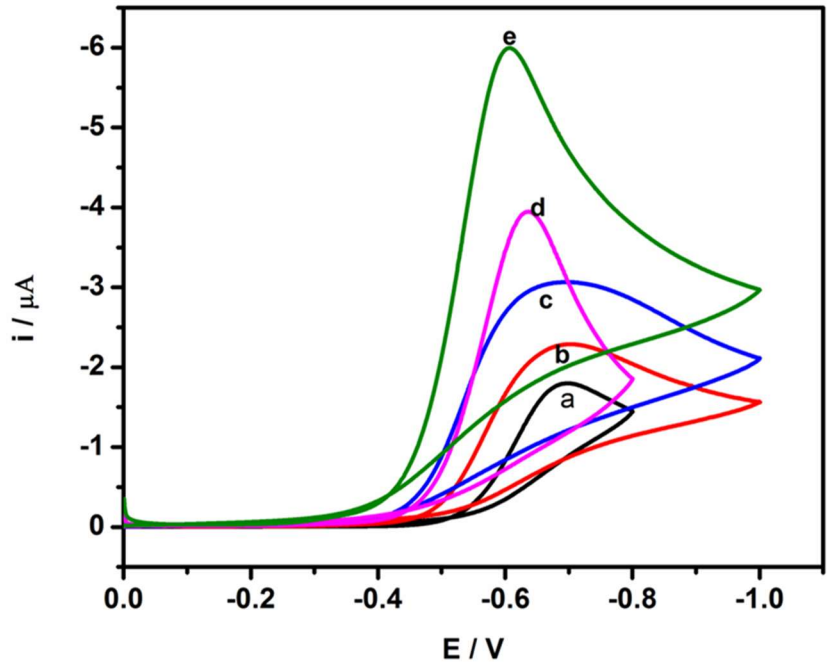

Figure 9. Cyclic voltammetric response of 10 µM nitrophenol on bare GCE (a) and $BiVO_4$ nanoparticles modified electrode pure (b), 1500 nm (c) 1200 nm (d) and 800 nm (e) in 2.5 pH B-R buffer solution at 100 mVs^{-1}.

The $BiVO_4$ nanoparticles offered superior electrocatalytic properties for the reduction of nitrophenol used on GCE to study bifenox herbicide reduction behavior. Figure 10a illustrates the cyclic voltammetric response of bifenox herbicide on bare GCE and modified $BiVO_4$ electrodes. As shown in Figure 10a, bifenox herbicide reduced on modified $BiVO_4$ electrode about -600 mV, and on bare GCE about -720 mV. A lower overpotential reduction can be observed on the $BiVO_4$ nanoparticles-modified electrode, as evidenced by the lower overpotential reduction. Further, a higher sensing current was observed on $BiVO_4$/GCE, indicating better electrocatalytic properties. The effect of the scan rate was investigated to determine whether the reaction was controlled by diffusion or adsorption (Figure 10b). A linear relationship was found between the square root of the scan rate and peak current, as shown in Figure 10c, indicating that diffusion controls the

reaction.[51] There are no reverse peaks in both bare and modified electrodes, indicating that bifenox undergoes irreversible reduction. To understand the number of electrons transferred in the reduction reaction and the kind of product formed, it is necessary to examine the reduction mechanism of bifenox. When the pH of the background electrolyte increased, the peak current increased, and a linear relationship was found between peak potential and pH, as depicted in Figure 8b with a slope of 68 mV/pH, indicating equal numbers of protons and electrons are involved in the reaction. The number of electrons transferred was calculated using the Randles-Sevcik equation by assuming the diffusion coefficient as 1.06 x10-5 $cm^{-2}s^{-1}$ [52], which was found to be 4.

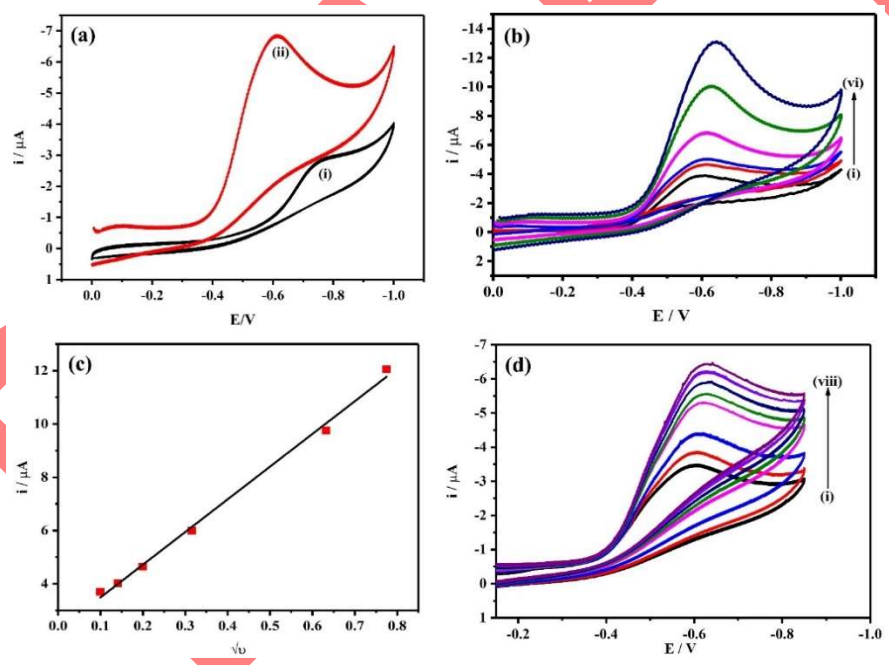

Figure 10. Cyclic voltammetric response of 10 µM bifenox on (a) bare GCE (i) and $BiVO_4$ modified electrode (ii) in 2.5 pH B-R buffer solution at 100 mVs^{-1}, (b) at different sweep rates: i) 10, ii) 20, iii) 30, iv) 100, v) 200, and vi) 600 mVs^{-1}, and (d) at different concentrations of bifenox i) 2, ii) 4, iii) 5, iv) 7, v) 9, vi) 11, vii) 13, and viii) 15 µM, scan rate:100 mVs^{-1}

Hence, four protons and four electrons are involved in the reduction of the mechanism of bifenox herbicide. The following mechanism is proposed for reducing bifenox in a 2.5 pH B-R buffer solution. A reduction peak results from reducing the nitro group of bifenox into a hydroxylamine group through 4 e^-. The higher sensing current observed in this work would appeal to the development of commercial and portable sensors. The peak current also increased as bifenox concentration increased (Figure 10d). It's always preferable to use pulse voltammetric techniques for electrochemical sensing of analytes since there is minimal interference from charging currents. DPV experiments were conducted with optimized instrument settings.

Electrochemical Impedance Spectroscopy of Bare/GCE and $BiVO_4$/GCE electrodes was performed and were compared in Figure 11. The charge transfer resistance value of the $BiVO_4$-modified electrode (804 Ω) is slightly lower than that of the bare glassy carbon electrode (1093 Ω). This indicates that the modified electrode facilitates faster electron transfer.

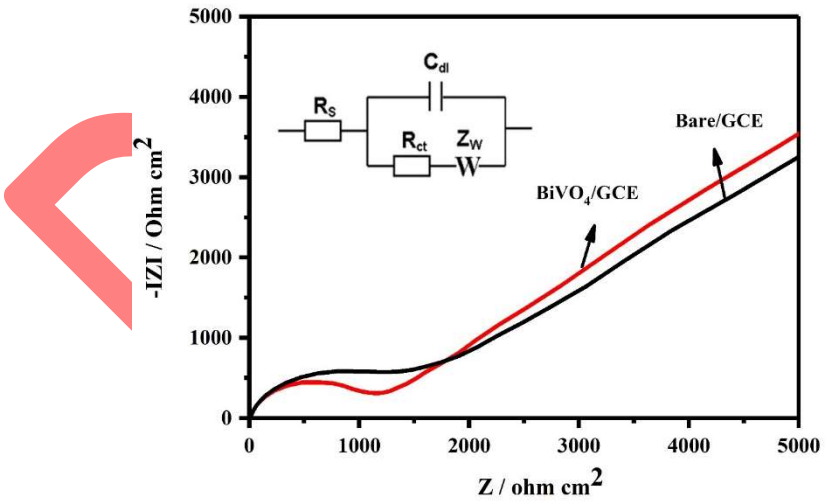

Figure 11. Comparative EIS analysis of Bare/GCE and $BiVO_4$/GCE.

The differential pulse voltammetric response of bifenox at various concentrations is illustrated in Figure 12a. A linear increase in peak current was observed when bifenox concentrations were increased from 0.1 to 20 nM, and the LOD was found to be 0.3 nM which

was calculated from the calibration curve by using the equation LOD = 3 s/m where s is the standard deviation of the intercept and m is the slope of the calibration curve.[53] According to the existing literature, this work achieves higher sensing current and lower detection limits.

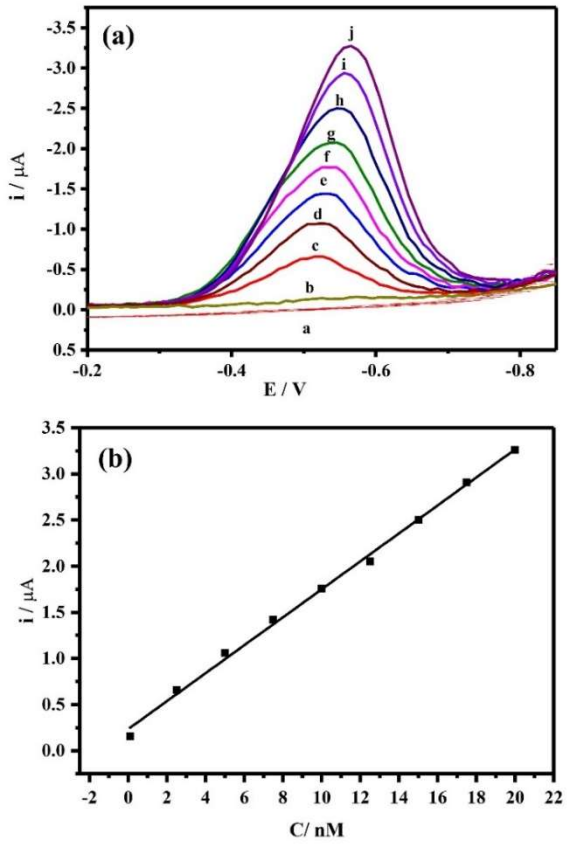

Figure 12. Differential pulse voltammetric response of bifenox at different concentrations: a) Nil, b) 0.1, c) 2.5, d) 5, e) 7.5, f) 10, g) 12.5, h) 15, i) 17.5 and j) 20 nM on $BiVO_4$/GCE in 2.5 pH B-R buffer solution (a) and Calibration graph (b).

3.8. Testing the reproducibility and stability of the bismuth vanadate modified GCE

Cyclic voltammetric experiments were carried out for 10 nM and were repeated seven times to ensure accuracy and precision. It was observed that peak currents were reproducible with a relative standard deviation of 2.8%. Figure 10a. In addition, the reproducible response and stability of the same electrode were examined. The electrode stability was investigated by

analyzing bifenox for 20 days using the same modified electrode Figure 13a. There was no significant change in peak current for 20 days, with a standard deviation of 2.1%. There was a gradual decline in the peak current after that. This may have been caused by the film's instability.

3.9. Electrochemical analysis of interfering ions and pesticides

The interferences caused by metal ions and other nitro compounds with the reduction signal of 2 nM bifenox were tested. The concentration of the metal ions and other pesticides added was 2 nM Figure 13b. This study found no interference between the inorganic cations and the other pesticides for the sensing signal. However, the reduction signal of bifenox is affected by adding 4-nitrophenol.

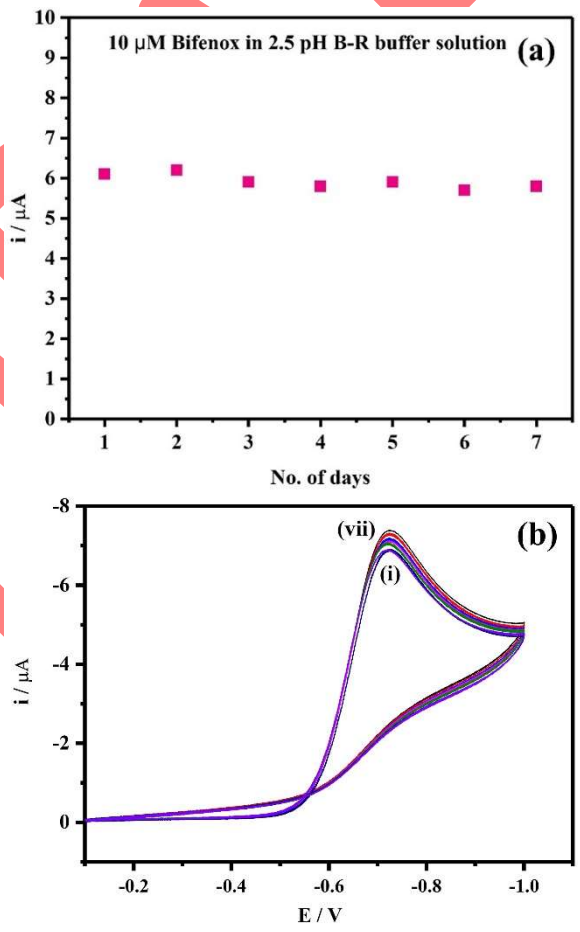

Figure 13. (a) Plot for peak current vs. number of days for 10 µM bifenox in 2.5 pH B-R buffer solution (b) Interference study of inorganic species and nitroaromatic pesticides such as (i) Na^{+}, (ii) Ca^{+}, (iii) Mg^{2+}, (iv) Parathion, (v) Methyl Parathion, (vi) Fenitrothion, and (vii) Chlorpyrifos, on the reduction signal of 10 µM bifenox at 100 mV s^{-1} in 2.5 pH B-R buffer solution at $BiVO_4$ modified GCE.

3.10. Determination of bifenox in water samples

The water was collected from the functional materials laboratory and analyzed for the presence of bifenox herbicide. It does not contain the bifenox. So the calculated amount of bifenox was spiked into the water sample. The bifenox from the water was extracted using dichloromethane. While extracting the bifenox from the water sample with dichloromethane, traces of water in the organic layer were present, which were removed with anhydrous sodium sulfate. After evaporation, the residue was dissolved in a pH 2.5 B-R buffer solution for electrochemical measurements. Table 2 and 3 summarizes the limit of detection obtained for previously reported methodologies and compares it with the current material. The comparison confirms the current size-controlled $BiVO_4$ materials show lower detection limits. Table 4 shows the $BiVO_4$ derives from hydrothermal method synthesis particles with different particle shapes. The current synthesis methodology allows size, shape, and surface to be easily controlled for a particular purpose.

Table 2: Comparison of the shape of the particles and electrochemical detection and reduction potential of synthesized $BiVO_4$ with previous reports.

Electrode Material	Shape of the material in study	Synthesis	Material for electrochemical detection	Limit of Detection (LOD)	Ref.
$BiVO_4$	Nano dendrites	Hydrothermal	Paraoxon	0.03 µM	[54]
$BiVO_4$	Porous structure	Solution Combustion	Acetaminophen	0.027 $\mu molL^{-1}$	[55]
$BiVO_4$	Spheres	Hydrothermal	Nitrite	1.5 $\mu molL^{-1}$	[56]
$BiVO_4$	Shuriken-flower shape	Solvent assisted Hydrothermal	Hexavalent Chromium (Cr VI)	0.035µM	[57]
$BiVO_4$	Clavate, Fusiform, Flowered, Bulky	Microwave approach	Paracetomol	0.2 µM	[58]
$BiVO_4$	Flake-ball	Sonochemical	Furazolidone	0.016 µM	[59]
$BiVO_4$	Microspheres	Co-precipitation	Rifampcin drug	0.014 µM	[60]
$BiVO_4$	Spheres	Hydrothermal	Bifenox	0.3 nM	This work

Table 3. Different materials comparison for electrochemical Bifenox detection

Electrode Material	Material for electrochemical detection	Limit of Detection (LOD)	Reduction Potential	Ref
$MnFe_2O_4$@CTS	Bifenox	0.09 $\mu molL^{-1}$	+0.23 V	BV1
$MnFe_2O_4$	Bifenox	-	-0.47 V	BV1
MWCNT	Bifenox	0.08 µM	+0.02 V	BV2
$BiVO_4$	Bifenox	0.3 nM	-0.61 V	This work

Table 4. Comparison of the shape and the applications of the Hydrothermally synthesized $BiVO_4$ nanoparticles with other works.

Synthesis route: Hydrothermal		
Shape of the nanoparticles	**Applications**	**Ref.**
Nanosheets	Photocatalyst	61
Bi-pyramidal microcrystals and Platelet microcrystals	Photocatalytic conversion from methane to methanol	62
Star-like shape	Methylene blue removal	63
Microsphere to regular decahedron	Controlled morphological studies	64
Sphere, star, cubic, and flower-like structures	Photocatalyst	65
Sphere, Lamellar structure	Photocatalytic O2 evaluation	66
Egg shape	Photocatalytic desulfurization of thiophene	67
Square sheet, leaf like Transparent spheres	Photocatalyst	68
Plate like nanostructure	Photocatalyst	69
Sphere to cubes	Supercapacitor	70
Spheres	Electrochemical detection of 4-nitrophenol and bifenox herbicide	This work

After the detection of bifenox herbicide, the $BiVO_4$ (1.5 mL Oleic acid) particles phase structure and morphology were analyzed using XRD and SEM. Figure 13 shows the XRD spectra of $BiVO_4$ 1.5 ml oleic acid after the experiment. The diffraction peaks seem to agree with the XRD pattern of the as-synthesized sample before the experiment. The slight variation in peak intensity

and broadness might be due to the etching process during the experiment. The SEM images of $BiVO_4$ 1.5ml oleic acid recovered after the electrochemical experiment are depicted in Figure 14. The spherical shape of the particles was retained with some disorders. The size of some particles was observed to be reduced, which might occur due to surface etching during the experiment. The EDS spectrum in Figure 14(d) shows the presence of Bi, V and O atoms in the synthesized sample after the experiment. Thus, the XRD and SEM analysis confirms that the structure and surface morphology of $BiVO_4$ particles were not changed greatly after the electrochemical detection experiment.

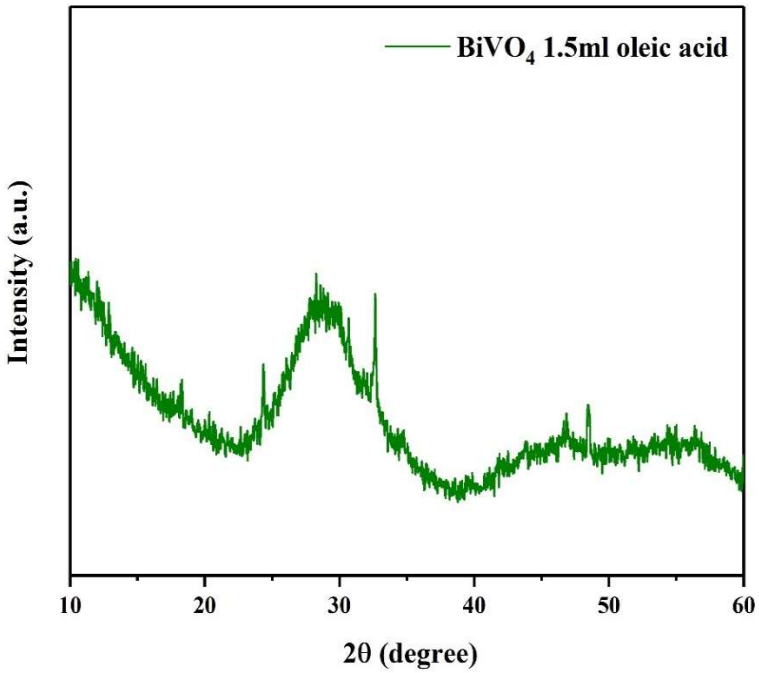

Figure 13. XRD pattern of $BiVO_4$ with 1.5 ml of oleic acid particles collected after the experiment

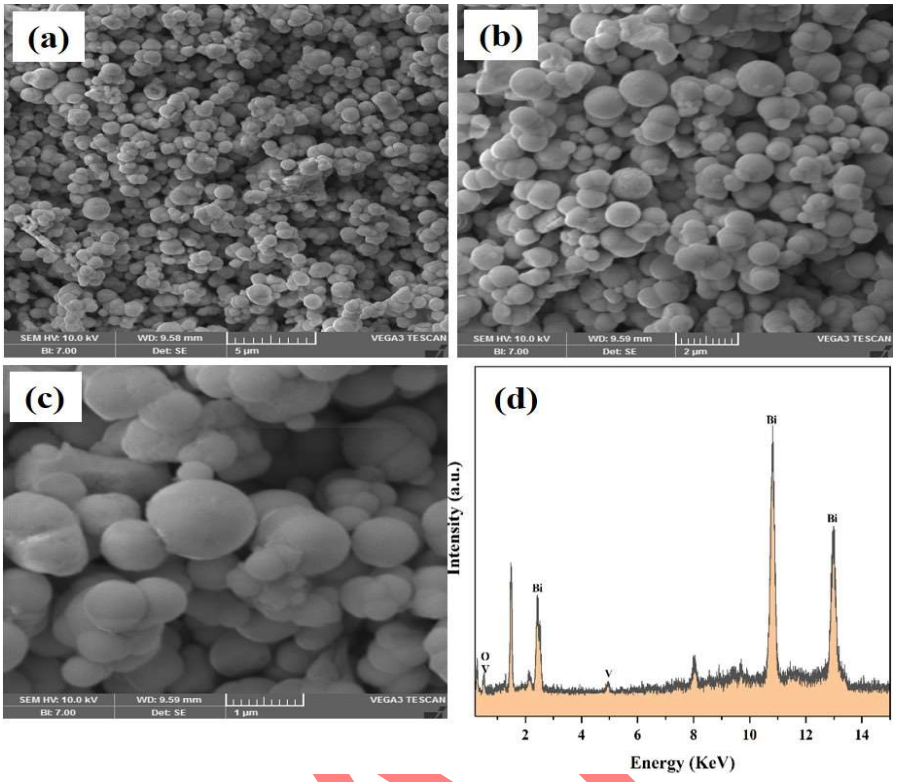

Figure 14. SEM images (a-c) and EDS spectrum (d) of $BiVO_4$ with 1.5 ml of oleic acid particles collected after the experiment

The particle size of the catalyst plays a predominant role in the electrochemical detection of pesticides and herbicides. Sensing capacity increased with the reduction of particle size of the catalyst due to the surface-to-volume ratio increase in the nanoparticle catalyst. Robin Chandra Boro et al. reported that gold nanoparticles catalyzed the detection of herbicide 2,4-dichlorophenoxyacetic acid with different particle sizes, and particle sensitivity was increased with decreasing particle size of the gold particle. **(SZ 1)** The same scenario was reflected in the present result while the sensitivity is increasing in decreasing the size of $BiVO_4$ particles.

4. Conclusion

$BiVO_4$ smooth surface spheres with periodic size reduction were achieved via the hydrothermal method. The morphology of $BiVO_4$ turns a smooth surface upon adding oleic acid

as an additive in the synthesis. XRD confirms the highly crystalline nature of the as-synthesized nanoparticles. Raman analysis denotes the shift in peaks with an increase in oleic acid concentrations. Smooth surface and periodic particle size reduction of synthesized $BiVO_4$ particles were observed with SEM analysis. A modified bismuth vanadate electrode has been developed to detect bifenox herbicide. Electrochemical results indicated that fabricated $BiVO_4$ modified electrode has a lower reduction potential, a higher sensing current, and better electrocatalytic activity. The $BiVO_4$-modified electrode shows a lower detection limit and reduction potential compared to previous reports. The BiVO4-based electrode is highly stable, which makes it possible to detect bifenox for up to seven experimental days without losing sensitivity. From the analysis report, this sensor can be easily used for field analysis. Its analytical validity was tested using spiked water samples, opening up new possibilities for environmental herbicide sensing.

Declaration

There is no conflict of interest; if accepted, the article will not be published elsewhere in the same form, in any language, without the publisher's written consent.

Data availability statement

Data will be made available on reasonable request.

Competing Interests

The authors have no relevant financial or non-financial interests to disclose.

Authorship contribution statement

Thangaraju Dheivasigamani **:** Conceptualization, Visualization, Methodology, Supervision, Writing - review & editing.

Kumaravel Ammasai: Electrochemical analysis, Methodology.

Govarthini Seerangan Selvam: Visualization, Writing - review & editing.

Priyadharshini Shanmugam**:** Visualization, Writing - original draft.

Durairajan Arulmozhi: Writing - review & editing.

References:

1 M. Zhang, C. Shao, X. Zhang and Y. Liu, *CrystEngComm*, 2015, **17**, 7276–7282.

2 Y. Geng, P. Zhang and S. Kuang, *RSC Adv.*, 2014, **4**, 46054–46059.

3 Y. Lu, Y. Pu, J. Wang, C. Qin, C. Chen and H. J. Seo, *Appl. Surf. Sci.*, 2015, **347**, 719–726.

4 H. Yi, L. Qin, D. Huang, G. Zeng, C. Lai and X. Liu, *Chem. Eng. J.*, 2019, **358**, 480–496.

5 P. Shanmugam, T. Dheivasigamani, S. Moorthy Babu, M. Shkir, E. El Sayed Massoud, R. Marnadu and V. R. Minnam Reddy, *Inorg. Chem. Commun.*, 2022, **146**, 110163.

6 B. Shunmughananthan, T. Dheivasigamani, J. Sthevan Kovil Pitchai and S. Periyasamy, *Dalt. Trans.*, 2022, **51**, 15579–15592.

7 W. W. Liu and R. F. Peng, *J. Electron. Sci. Technol.*, 2020, **18**, 119–137.

8 P. Wang, W. Ji, M. Li, G. Zhang and J. Wang, *Ultrason. Sonochem.*, 2017, **38**, 289–297.

9 X. Zhao, Z. Duan and L. Chen, *Ind. Eng. Chem. Res.*, 2019, **58**, 10402–10409.

10 M. Song, Y. Wu, C. Xu, X. Wang and Y. Su, *J. Hazard. Mater.*, 2019, **368**, 530–540.

11 Z. Zhang, X. Sun and M. Dresselhaus, *Phys. Rev. B*, 2000, **61**, 4850–4861.

12 M. Rohloff, B. Anke, S. Zhang, U. Gernert, C. Scheu, M. Lerch and A. Fischer, *Sustain. Energy Fuels*, 2017, **1**, 1830–1846.

13 Y. Park, K. J. Mc Donald and K. S. Choi, *Chem. Soc. Rev.*, 2013, **42**, 2321–2337.

14 S. Ghotekar, K. Pagar, S. Pansambal, H. C. A. Murthy and R. Oza, *Adv. J. Sci. Eng.*, 2020, **1**, 104–110.

15 S. Bai, K. Tian, N. Han, J. Guo, R. Luo, D. Li and A. Chen, *Inorg. Chem. Front.*, 2020, **7**, 1026–1033.

16 Y. Zhang, Y. Guo, H. Duan, H. Li, C. Sun and H. Liu, *Phys. Chem. Chem. Phys.*, 2014, **16**, 24519–24526.

17 S. Gu, W. Li, F. Wang, S. Wang, H. Zhou and H. Li, *Appl. Catal. B Environ.*, 2015, **170**–**171**, 186–194.

18 S. Obregón, A. Caballero and G. Colón, *Appl. Catal. B Environ.*, 2012, **117**–**118**, 59–66.

19 A. Kudo, K. Omori and H. Kato, *J. Am. Chem. Soc.*, 1999, **121**, 11459–11467.

20 K. K. Dey, S. Gahlawat and P. P. Ingole, *J. Mater. Chem. A*, 2019, **7**, 21207–21221.

21 M. Ganeshbabu, N. Kannan, P. S. Venkatesh, G. Paulraj, K. Jeganathan and D. MubarakAli, *RSC Adv.*, 2020, **10**, 18315–18322.

22 Z. Wang, X. Huang and X. Wang, *Catal. Today*, 2019, **335**, 31–38.

23 R. Liu, J. Ren, D. Zhao, J. Ning, Z. Zhang, Y. Wang, Y. Zhong, C. Zheng and Y. Hu, *Inorg. Chem. Front.*, 2017, **4**, 2045–2054.

24 M. F. R. Samsudin, S. Sufian and B. H. Hameed, *J. Mol. Liq.*, 2018, **268**, 438–459.

25 Z. Liang, Y. Cao, H. Qin and D. Jia, *Mater. Res. Bull.*, 2016, **84**, 397–402.

26 C. Ravidhas, A. Juliat Josephine, P. Sudhagar, A. Devadoss, C. Terashima, K. Nakata, A. Fujishima, A. Moses Ezhil Raj and C. Sanjeeviraja, *Mater. Sci. Semicond. Process.*, 2015, **30**, 343–351.

27 Y. Lin, C. Lu and C. Wei, *J. Alloys Compd.*, 2019, **781**, 56–63.

28 T. Kansaard and W. Pecharapa, *Ferroelectrics*, 2019, **552**, 140–147.

29 N. Sumathi, A. C. Dhanemozhi, D. Thangaraju, S. A. Adewinbi, K. Mohanraj, R.

Marnadu and M. Shkir, *Surfaces and Interfaces*, 2021, **26**, 101408.

30 T. Gupta, Samriti, J. Cho and J. Prakash, *Mater. Today Chem.*, 2021, **20**, 100428.

31 R. Karthikeyan, M. Navaneethan, J. Archana, D. Thangaraju, M. Arivanandhan and Y. Hayakawa, *Dalt. Trans.*, 2014, **43**, 17445–17452.

32 A. Jabłońska-Trypuć, E. Wołejko, U. Wydro and A. Butarewicz, *J. Environ. Sci. Heal. - Part B*, 2017, **52**, 483–494.

33 M. E. DeLorenzo, G. I. Scott and P. E. Ross, *Environ. Toxicol. Chem.*, 2001, **20**, 84–98.

34 A. Jabłońska-Trypuć, U. Wydro, L. Serra-Majem, E. Wołejko and A. Butarewicz, *Int. J. Environ. Res. Public Health*, 2019, **16**, 4137.

35 A. T. K. Tran, R. V Hyne and P. Doble, *Chemosphere*, 2007, **67**, 944–953.

36 Y. Wang, X. Jin, D. Zhao, X. Guo and R. Li, *Anal. Methods*, 2015, **7**, 6411–6418.

37 N. Song, J. Y. Lee, A. R. Mansur, H. W. Jang, M. Lim, Y. Lee, M. Yoo and T. G. Nam, *Food Chem.*, 2019, **298**, 125050.

38 E. Calvaruso, G. Cammilleri, A. Pulvirenti, G. M. Lo, G. Lo Cascio, V. Giaccone, V. V. Badaco, M. M. Alessandra, A. Vella, A. Macaluso, D. Bella, V. Ferrantelli, G. Lo Cascio, V. Giaccone, V. V. Badaco, V. Ciprì, M. Maria, A. Vella, A. Macaluso, C. Di Bella and V. Ferrantelli, *Nat. Prod. Res.*, 2020, **34**, 34–38.

39 R. Madhu, C. Karuppiah, S. M. Chen, P. Veerakumar and S. Bin Liu, *Anal. Methods*, 2014, **6**, 5274–5280.

40 B. Wu, S. Yeasmin, Y. Liu and L. J. Cheng, *Sensors Actuators B Chem.*, 2022, **354**, 131216.

41 J. Mao, Q. Wu, F. Tao, W. Xu, T. Hong and Y. Dong, *RSC Adv.*, 2020, **10**, 6395–6404.

42 F. Lin, D. Wang, Z. Jiang, Y. Ma, J. Li, R. Li and C. Li, *Energy Environ. Sci.*, 2012, **5**, 6400–6406.

43 A. P. Jadhav, C. W. Kim, H. G. Cha, A. U. Pawar, N. A. Jadhav, U. Pal and Y. S. Kang, *J. Phys. Chem. C*, 2014, **118**, 14060.

44 Q. Luo, L. Zhang, X. Chen, O. K. Tan and K. C. Leong, *RSC Adv.*, 2016, **6**, 15796–15802.

45 O. F. Lopes, K. T. G. Carvalho, G. K. Macedo, V. R. de Mendonça, W. Avansi and C. Ribeiro, *New J. Chem*, 2015, **39**, 6231–6237.

46 T. D. Nguyen, Q. T. P. Bui, T. B. Le, T. M. Altahtamouni, K. B. Vu, D. V. N. Vo, N. T. H. Le, T. D. Luu, S. S. Hong and K. T. Lim, *RSC Adv.*, 2019, **9**, 23526–23534.

47 L. Wang, X. Gu, Y. Zhao, M. Wei, Y. Qiang and Y. Zhao, *J. Mater. Sci. Mater. Electron.*, 2018, **29**, 19278–19286.

48 Y. Chen, Y. Liu, X. Xie, C. Li, Y. Si, M. Zhang and Q. Yan, *J. Mater. Sci. Mater. Electron.*, 2019, **30**, 9311–9321.

49 Z. Zhang, M. Wang, W. Cui and H. Sui, *RSC Adv.*, 2017, **7**, 8167–8177.

50 A. Kumaravel and M. Murugananthan, *Sensors Actuators, B Chem.*, 2021, **331**, 129467.

51 H. Salehzadeh, M. Ebrahimi, D. Nematollahi and A. A. Salarian, *J. Electroanal. Chem.*, 2016, **767**, 188–194.

52 A. Kumaravel and M. Chandrasekaran, *Sensors Actuators B. Chem.*, 2012, **174**, 380–388.

53 A. Kumaravel and M. Chandrasekaran, *Sensors Actuators, B Chem.*, 2011, **158**, 319–326.

54 P. K. Gopi, D. B. Ngo, S. M. Chen, C. H. Ravikumar and W. Surareungchai, *Chemosphere*, 2022, **288**, 132511.

55 M. da Silva Araújo, T. R. Barretto, J. C. R. Galvão, C. R. T. Tarley, L. H. Dall'Antônia, R. de Matos and R. A. Medeiros, *Electroanalysis*, 2021, **33**, 663–671.

56 F. Wirley, P. Ribeiro, F. Cruz, E. Chaves, F. Marken and L. Helena, *Electrochem. commun.*, 2015, **61**, 1–4.

57 D. Prabu, B. Thirumalraj and S. Chen, *J. Hazard. Mater.*, 2019, **367**, 647–657.

58 Y. Liu, X. Xu, C. Ma, F. Zhao and K. Chen, *Nanomaterials*, 2022, **12**, 1173.

59 C. Koventhan, S. Pandiyarajan and S. M. Chen, *J. Alloys Compd.*, 2022, **895**, 162315.

60 V. Vinothkumar, A. Sangili, S. M. Chen and M. Abinaya, *Colloids Surfaces A Physicochem. Eng. Asp.*, 2021, **624**, 126849.

61 L. Zhang, D. Chen and X. Jiao, *J. Phys. Chem. B*, 2006, **110**, 2668–2673.

62 W. Zhu, M. Shen, G. Fan, A. Yang, J. R. Meyer, Y. Ou, B. Yin, J. Fortner, M. Foston, Z. Li, Z. Zou and B. Sadtler, *ACS Appl. Nano Mater.*, 2018, **1**, 6683–6691.

63 S. Sun, W. Wang, L. Zhou and H. Xu, *Ind. Eng. Chem. Res.*, 2009, **48**, 1735–1739.

64 Y. Zhao, R. Li, L. Mu and C. Li, *Cryst. Growth Des.*, 2017, **17**, 1528–7483.

65 H. Fan, D. Wang, L. Wang, H. Li, P. Wang, T. Jiang and T. Xie, *Appl. Surf. Sci.*, 2011, **257**, 7758–7762.

66 D. Ke, T. Peng, L. Ma, P. Cai and K. Dai, *Inorg. Chem.*, 2009, **48**, 4685–4691.

67 M. M. Kamazani, *J. Mater. Sci. Mater. Electron.*, 2019, 1–6.

68 Y. Shen, M. Huang, Y. Huang, J. Lin and J. Wu, *J. Alloys Compd.*, 2010, **496**, 287–292.

69 G. Xi and J. Ye, *Chem. Commun.*, 2010, **46**, 1893–1895.

70 R. Packiaraj, K. S. Venkatesh, P. Devendran, S. A. Bahadur and N. Nallamuthu, *Mater. Sci. Semicond. Process.*, 2020, **115**, 105122.